Dynamic Shear Rheology and Structure Kinetics Modeling of a Thixotropic Carbon Black Suspension

Matthew J. Armstrong[1], Antony N. Beris[2], Simon A. Rogers[3], and Norman J. Wagner[2,4]

Center of Molecular and Engineering Thermodynamics
Department of Chemical and Biomolecular Engineering,
University of Delaware, Newark, DE 19716

Created on 5MAR17
Last edited by MJA 5MAR17
In preparation for submission to Rheologica Acta

Abstract The rheological characterization of a model, nearly ideal thixotropic carbon black suspension first proposed by Dullaert and Mewis (JNNFM 139: 21-30, 2006) is extended to include large amplitude oscillatory shear (LAOS) flow, shear flow reversal, unidirectional LAOS flow (UD-LAOS). We show how this broader data set is useful for validating and improving constitutive models of thixotropy. We apply this new data to further test a recently developed structure-kinetics model, the Modified Delaware Thixotropy Model, (Armstrong et al. J Rheol. 60: 433-450, 2016) as well as to better understand the microstructural basis and validity of strain rate superposition methods proposed with the framework of soft glassy rheology (SGR) modeling. This comparison identifies the limitations of models based on a scalar description of microstructure, which cannot fully capture the reversal of flow directionality inherent in LAOS flow. Further, we use the model to identify a possible microstructural justification for the hypothesized technique of strain rate superposition in the SGR model.

[1] Present address: Department of Chemistry and Life Science, United States Military Academy, West Point, New York 10996.

[2] Present address: Center for Molecular and Engineering Thermodynamics, Department of Chemical and Biomolecular Engineering, University of Delaware, Newark, Delaware 19716

[3] Present address: Department of Chemical and Biomolecular Engineering, University of Illinois Urbana-Champaign, Champaign, Illinois 61801.

[4] Corresponding Author. Tel. +001 302- 831-8079

E-mail address: wagnernj@udel.edu

Keywords Carbon black · Thixotropy · Large amplitude oscillatory shear · Constitutive modeling

Introduction

The present work focuses on a broad rheological characterization of a model thixotropic suspension comprised of 3.23% carbon black in napthenic oil, the ability of a recent structure-kinetics model of thixotropy to fit and predict the rheology, and the validity of strain rate superposition analysis proposed within soft glassy rheology (SGR) (Apostolidis et al. 2015; Armstrong 2015; Wyss 2007; Armstrong et al. 2016a). This particular carbon black system was formulated and characterized by Dullaert and Mewis (2005a; 2006), and Dullaert (2005), and used to validate thixotropy models by Dullaert and Mewis (2005a; 2006). Many additional carbon black systems have been researched and published by Youssry et al. (2013), Amari and Watanabe (1990), Aoki (2011a; 2011b), Aoki and Watanabe (2004), Aoki et al. (2003a; 2003b) and Yearsley et al. (2012) demonstrating that the carbon black system remains relevant, interesting and rheologically significant.

Carbon black is germane to many industrial processes, such as for reinforcing rubber products, for pigmentation in inks, as well as for providing conductivity (Metzner and Whitlock 1958; Russel 1980; Amari and Watanabe 1990; Aoki et al. 2003a; Dullaert 2005; Yearsley et al. (2012); Youssry et al. 2013). Consequently, extensive studies of the linear viscoelastic properties of carbon black suspensions of various source and in various solvents can be found in the literature (e.g. Aoki et al. 2003a; 2003b). Because of the industrial importance and the complex relationships between the nanoscale and microscale structure, processing, and rheology, there is a need to have a well-defined reference system that is reproducible between laboratories for use in scientific investigations. Dullaert and Mewis (2005a; 2006) proposed and published a nearly ideal thixotropic system of a commercial carbon black in napthenic oil suspension. Careful sample preparation produced a sample with reversible and reproducible thixotropy. With this system, they investigated stress jumps, steady state, and transient shear rheology. Stress jump measurements identified elastic stresses present during steady state flow that were directly attributable to the carbon microstructure present, which was shown to be a function of the current shear rate (Dullaert 2005; Dullaert and Mewis 2005a; Dullaert and Mewis 2005b; Dullaert and Mewis 2006; Mewis and Wagner 2012). This data set was used to further the development of structure kinetics models for thixotropy, incorporating elastic and viscous contributions to the total stress that depend on a time and shear rate dependent structure parameter (Mujumdar et al. 2002; Dullaert and Mewis 2006; Mewis and Wagner 2012; Dimitriou 2013).

Contemporary work on thixotropy modeling using a structure-kinetics approach includes a wide variety of approaches, e.g., Mewis and Wagner (2009), Mewis and Wagner (2012), de Souza and Thompson (2012; 2013), Dimitriou et al. (2013), Larson (2015) and Armstrong et al. (2016a). The Dullaert and Mewis structural kinetics model for thixotropy has been the basis of "Type I" models as defined by de Souza and Thompson (de Souza and Thompson 2012; de Souza and Thompson 2013). Work to evolve Bingham-like constitutive models that incorporate a structure parameter include contributions by Mujumdar et al. (2002) and more recently, Yearsley et al. (2012). Meanwhile, Osuji et al. (2008) reported simultaneous optical and rheological investigations to link the elasticity in carbon black suspensions to the floc structure. Clearly, a significant research focus is to develop a quantitative, microstructural understanding that can ultimately be used for the rational formulation of thixotropic, carbon black suspensions.

There is also significant interest in using large amplitude oscillatory shear (LAOS) to study material properties and potentially, for determining parameters in rheological constitutive models (Hyun et al. 2011, Rogers et al. 2011; Germann et al. 2016). Consequently, we extend the model system data set of Dullaert and Mewis (Dullaert 2005; Dullaert and Mewis 2006) to include measurements of LAOS and a related method, Uni-Directional Large Amplitude Oscillatory Shear (UD-LAOS) (Armstrong et al. 2016a). We use this new, extended data set to rigorously test the ability of a structure kinetics model (the Modified Delaware Thixotropic (MDT) model) to predict the LAOS and UD-LAOS behavior over a broad range of frequency and amplitude. In the following, we provide a description of the model carbon black system and its preparation, along with a summary of the MDT model and a brief description of the model parameter fitting algorithm. Rheological experimental results and model fits will be presented next, followed by tests of model predictions for LAOS and UD-LAOS. Finally, the extended data set and model predictions are used to explore the hypothesis of strain rate superposition as discussed by Wyss et al. (2007).

Materials, Methods, and Experimental Protocol

A model thixotropic suspension reported by Dullaert and Mewis (2005a, 2006) was reformulated for this work, following as closely as possible the prescribed methods. The suspension consists of 3.23 vol% Carbon black (FW2, Orion Engineered Carbons LLC, Kingwood TX) aggregates with primary particle radius of 13nm in naphthenic oil, (American Chemical, density SG = 0.983; η =1.70 Pa s; C_{20}-C_{50} chains: MW=282-702 g/mol). Note that the exact naphthenic oil differs slightly from that used by Dullaert and Mewis (2006) (Shell, SG = 0.98; η =1.41 Pa s), due to availability. The particles were dispersed in the blended solution using a Silverson, model L4Rt mixer with the tubular mixing unit with square hole high shear screen operating at 8000 rpm for 30 minutes. This was followed by degassing at 40^{o}C in a vacuum chamber for 1 hour. Samples were stored on the Wheaton benchtop roll-mixer.

The rheological measurement protocol followed was identical that followed in Dullaert and Mewis (2006) and extended to the additional tests by Armstrong et al. (2016a), such that only a summary is provided here. All of the rheological measurements were performed with the ARES G2 strain controlled rheometer (TA Instruments) using a 50mm cone and plate geometry with a cone angle of 0.0404 rad (Armstrong et al. 2016a). Measurements of the steady state stress were performed after a preshear of 300 (s^{-1}) for 300s, and an adequate equilibration time that was dependent upon the shear individual steady state shear rate varying between 10 min for the highest shear rates tested (300 s^{-1}) and 2 hours for the smallest shear rates tested (10^{-3} s^{-1}) (Armstrong

2015; Armstrong et al. 2016a). The transient step-up and step-down experiments, as well as all of the LAOS experiments were preceded by a preshear of 300 (s^{-1}) for 300 s, followed by a period of time to arrive at a steady stress value for a given initial shear rate (600–900 s for all shear rates) (Armstrong 2015; Armstrong et al. 2016a). The viscosities measured during each preshear test were checked between each experiment to determine that no irreversible changes occurred to the sample during testing. The elastic stress was measured using a strain jump experiment following the procedure outlined by Dullaert and Mewis and the details are shown in the Supplementary Material Fig. S.2a (Dullaert 2005; Dullaert and Mewis 2005a; Armstrong 2015; Armstrong et al. 2016a).

Comparisons to the literature rheological data validate the reproducibility of the system between laboratories and are shown in the Supplemental Material. The steady shear viscosity compares well with that reported by Dullaert and Mewis (Dullaert 2005; Dullaert and Mewis 2005a), where a small quantitative difference is attributed to the difference in the background viscosity of the suspending fluid blend ($1.7\ \mathrm{Pa \cdot s}$ here in comparison with $1.4\ \mathrm{Pa \cdot s}$ reported by Dullaert and Mewis). Furthermore, the elastic stress component of total stress also compares well with the Dullaert and Mewis system, where the stress jump data (used to calculate the elastic stress components shown) are shown in Figure S.2a in the Supplemental Material (Dullaert 2005; Dullaert and Mewis 2005a; Dullaert and Mewis 2005b; Dullaert and Mewis 2006; Armstrong 2015; Armstrong et al. 2016a).

Modified Delaware Thixotropic Model Summary

The Modified Delaware Thixotropic model (MDT) used to fit and predict the rheological data in this manuscript is a thixotropic, scalar structure-kinetics model developed from the framework put forth originally by Goodeve (1939) and built upon by Mujumdar et al. (2002). It is derived and discussed in detail in a recent publication (Armstrong et al., 2016a), so only the key working equations are summarized here.

The stress, σ_{tot} is postulated to be comprised of a sum of an elastic σ_e and viscous σ_v component:

$$\sigma_{tot} = \sigma_e(\lambda) + \sigma_v(\lambda) \ , \tag{1}$$

both functions of a scalar structure parameter λ, spanning [0 1], where 0 represents no microstructure, and 1 represents complete structuring of the material. More specifically we have

$$\begin{aligned} \sigma_e(\lambda) &= G_f(\lambda)\gamma_e(\lambda) \\ \sigma_v(\lambda) &= \lambda K_{ST}\dot{\gamma}_p(\lambda)^{n_2} + K_\infty \dot{\gamma}_p(\lambda)^{n_1} \end{aligned} \ , \tag{2}$$

where G_f is the elastic modulus, γ_e is the elastic strain, $\dot{\gamma}_p$ the plastic strain rate, and K_{ST} K_∞ are the consistency parameters, while n_1 and n_2 are the corresponding power law indices (Mujumdar et al. 2002; Dullaert and Mewis 2006; Mewis and Wagner 2012; Armstrong 2015; Armstrong et al. 2016a). Note that the total strain, γ (and, correspondingly, the total shear rate, $\dot{\gamma}$) is decomposed within the MDT model into an elastic, γ_e (correspondingly $\dot{\gamma}_e$) and a plastic, γ_p (correspondingly $\dot{\gamma}_p$) contributions

$$\gamma = \gamma_e + \gamma_p \quad \Leftrightarrow \quad \dot{\gamma} = \dot{\gamma}_e + \dot{\gamma}_p \ . \tag{3}$$

The concept of breaking strain and shear rate into elastic and plastic components was introduced by Dimitriou et al. (2013), following ideas from the theory of kinematic hardening in the description of plasticity, and was modified by Armstrong et al. (2016a). It leads to the following calculation for the plastic shear rate

$$\dot{\gamma}_p = \begin{cases} \dfrac{\dot{\gamma}}{\left(2 - \dfrac{|\gamma_e|}{\gamma_{\max}}\right)} & \dot{\gamma} \geq 0 \\[2ex] \dfrac{\dot{\gamma}}{\left(2 + \dfrac{|\gamma_e|}{\gamma_{\max}}\right)} & \dot{\gamma} < 0 \end{cases} \ , \tag{4}$$

where $\gamma_{\max}$ represents the fully structured, maximum value of elastic strain before rupture of the structure that is given by

$$\gamma_{\max} = \min\left(\frac{\gamma_y}{\lambda^m}, \gamma_\infty\right) \tag{5}$$

where γ_y, γ_∞, are the critical strain at yield, infinite shear shear stress, respectively. Corresponding to Eqs. (3) and (4) the following equation can be extracted describing the rate of change of the elastic strain

$$\frac{d\gamma_e}{dt} = \dot{\gamma}_p - \frac{\gamma_e}{\gamma_{\max}}\left|\dot{\gamma}_p\right|. \tag{6}$$

The MDT model involves two more ordinary differential equations in addition to Eq. (6), one for the structure evolution, λ, and one for the elastic modulus evolution, G_f. The evolution equation for the scalar structural parameter, λ is

$$\frac{d\lambda}{dt} = k_{Brown}\left[-\lambda\left|\hat{t}_{r1}\dot{\gamma}_p\right|^a + (1-\lambda)\left(1+\left|\hat{t}_{r2}\dot{\gamma}_p\right|^d\right)\right], \tag{7}$$

where k_{Brown} is structural breakage constant with units of inverse time, while $\hat{t}_{r1}$ and $\hat{t}_{r2}$ are dimensionless thixotropic time constants, a and d, are fitting parameters. The elastic modulus evolution equation is

$$\frac{dG_f}{dt} = -k_G\left(G_f - \lambda G_0\right), \tag{8}$$

where k_G is the time constant associated with the evolution of the current value of elastic modulus, and G_0 represents the elastic modulus of the fully structured material. The model parameters and their values are summarized in Table 1. As mentioned, in our fit to the data, the optimized value of γ_∞ was determined to be 1

The parameters of the Modified Delaware Thixotropic model were fit to the data measured for Linear Viscoelasticity (LVE), steady shear, and step-up/down experiments following the procedure outlined in Armstrong et al. 2016a. The first five parameters of the MDT model ($\sigma_{y0}, \eta_\infty, n_1, G, m$) were fit using steady state values at the limit of small and high shear rates and small oscillatory shear (SAOS) data. Keeping these first five parameter values constant, the remaining eight model parameters (shown in Table 1) are fit using a stochastic, parallel tempering algorithm that searches for a feasible pseudo-global minimum. The search involves the minimization of a user-defined objective function, F_{OBJ}, that represents an L_2 norm of the differences between the experimental data and the MDT model predictions scaled with respect to data

$$F_{OBJ} = \frac{1}{M}\sum_{k=1}^{M}\frac{1}{P_k}\left\|\frac{(\sigma_{Model} - \sigma_{Data})}{\sigma_{Data}}\right\|_{2,k} , \tag{9}$$

where P_k represents the number of points in the k-th data set, and M is the total number of data sets. For the parameter fits we used the steady state data, the elastic stress, and 16 different step-up and step down transient data sets. This novel parallel tempering algorithm is described in more detail in (Armstrong 2015; Armstrong et al. 2016b).

From the results of 10 independent trials, statistics were calculated, including parameter averages, and standard deviations. These are tabulated in Table 1, and are presented along with the average and standard deviation of the resulting 10 independent fits. The MDT model always converged to a single basin with respect to F_{OBJ} as observed from the parameter values from the 10 trials.

Table 1: Parameter values fitting MDT model to carbon black system. Shaded parameters are determined from the LVE and steady shear rheology, while the remaining 8 parameters are determined by optimization to the 18 (total) data sets including all step-up and step-down experiments

Parameter	Units	Meaning	Range Initial Guess	Limiting Values	Optimal	Average	Range: (+/-)
σ_{y0}	Pa	Yield stress	(-)	>0	7.82	(-)	(-)
η_∞	Pa s^{n1}	Infinite shear viscosity	(-)	>0	2.9	(-)	(-)
n_1	(-)	Power law η_∞	(-)	>0	1	(-)	(-)
G_0	Pa	Elastic Modulus	(-)	>0	1600	(-)	(-)
m	(-)	Power law parameter of γ_e evolution	(-)	[-2 2]	-1.5	(-)	(-)
γ_∞	(-)	Maximum allowable strain	(-)	~1	1	(-)	(-)
γ_y	(-)	Yield strain	(-)	[0 1]	$4.88e^{-3}$	(-)	(-)
K_{ST}	Pa s^{n2}	Consistency parameter	[20-25]	>0	10.42	10.5	0.45
n_2	(-)	Power law parameter K_{ST}	[.5 - 1]	[.5 - 1]	1.13	1.15	0.05
a	(-)	Power law parameter shear breakage	[1 - 2]	[1 - 2]	1.59	1.62	0.10
d	(-)	Power law parameter shear aggregation	[0.25 - 0.75]	[0.25 - 0.75]	0.68	0.70	0.02
k_{Brown}	s^{-1}	Characteristic time of Brownian motion	[$1e^{-3}$ - 1]	>0	0.055	0.052	0.05
$\hat{t}_{r1}$ $(k_{break}/k_{Brown})^{1/a}$	s	Characteristic time of λ breakdown	[$1e^{-3}$ - 1]	>0	0.74	0.70	0.05
$\hat{t}_{r2}$ $(k_{aggr}/k_{Brown})^{1/d}$	s	Characteristic time of λ buildup	[$1e^{-3}$ - 1]	>0	1.54	1.50	0.05
k_G	s^{-1}	Characteristic time of G evolution	[$1e^{-3}$ - 1]	>0	0.346	0.30	0.05

Experimental Results and Model Fitting

First, we discuss steady state and linear viscoelasticity experimental results that were used to determine the following parameters: $\sigma_{y0}, \eta_\infty, G_0, n_1, m, \gamma_y$. In Fig. 1a we compare the steady state total shear and elastic stresses as a function of the shear rate against the best fit of the MDT model over more than five orders of magnitude variation in shear rate. The data exhibit a significant yield stress at low shear rates and a subsequent shear thinning that leads to a nearly constant viscosity at high shear rates. The elastic component of this steady shear stress is observed to monotonically decrease with increasing shear rates as the structure is broken down by the flow. Both the total and elastic component of the shear stress are well fit by the MDT model consistent with other thixotropic systems observations (Armstrong 2015; Armstrong et al. 2016). An advantage of the MDT model is the extraction of microstructural information through the structure parameter lambda. Its behavior is also shown in Fig. 1a, confirming the trends described. The structure parameter remains close to 1 (fully structured) until the total stress rises above the yield stress or, correspondingly, the elastic stress starts decreasing, whereupon it drops to become asymptotically zero (fully unstructured) at the highest shear rates probed, commensurate with the loss of elasticity.

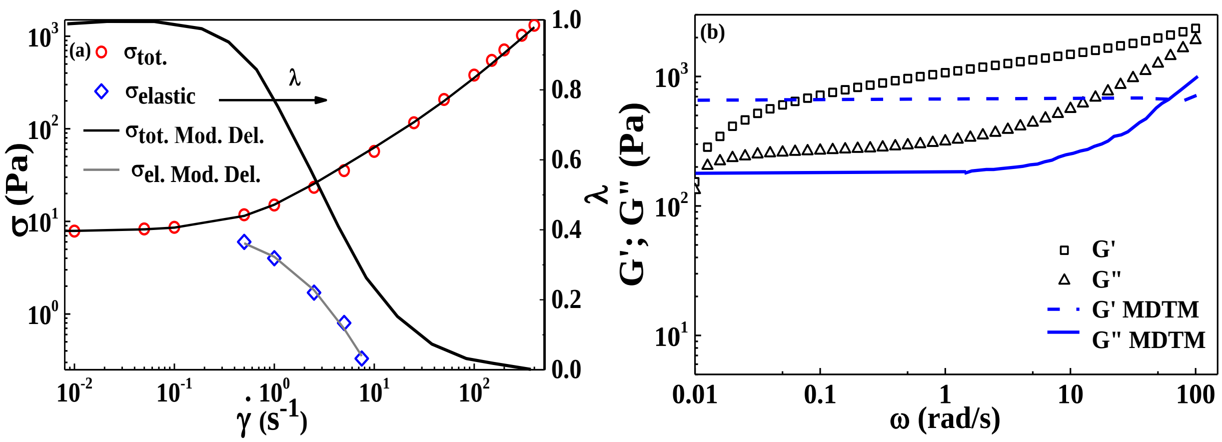

Fig. 1: (a) Steady state total stress and elastic shear stress (left axis) and structure parameter λ; (b) Storage (G') and Loss (G") moduli obtained in SAOS frequency sweep at $\gamma_0 = 0.01$. Open symbols: experimental data; Continuous and dashed lines: MDT model fits using the parameter values indicated in Table 1.

The linear viscoelastic properties of the fully structured suspension at rest are shown in Fig. 1b along with the fits obtained with the MDT model. The amplitude sweep experiment used to define the linear regime is shown in Supplemental Material (Fig. S.2b). Note that the experimental spectrum does not exhibit a terminal liquid regime at the lowest frequencies probed, but rather is characteristic of a material with an apparent yield stress. The elastic modulus, G_0 is determined from the MDT model to be constant at 1600 (Pa). This value is calculated from the relationship for the critical yield strain γ_y as the ratio of the yield stress and elastic modulus ($\gamma_y = \sigma_{y0}/G_0$). Amplitude sweep experiments (Figure S.2b in the Supplemental Material) show γ_y ~0.01, and the yield stress is determined from the steady shear experiments. This simple model fits the frequency dependent elasticity with a reasonable value for the elastic modulus and a better fit requires models for viscoelasticity (Armstrong 2015; Armstrong et al. 2016a). The loss modulus arises from viscous contributions to the stress, which are also frequency independent, as well as a viscous component, which is linear in the applied frequency and hence, evident at higher frequencies.

Two basic protocols are followed for the step up and step down in shear rate experiments. The first is transitioning to a common final value from different initial steady shear rate values, while the second is transitioning from a common initial steady shear rate to different final values. In both experiments, the initial state prior to the change in shear rate is steady such that the structure evolves from a well-defined state. It is also be important for a later discussion that these experiments are conducted without a change in flow direction. The results of the step up and step down experiments are shown in Fig. 2. Note that the initial stress values prior to the applied change in the shear rate correspond to points on the steady flow curve (Fig. 1a) and only the transient stress responses after the time of the rate jump is applied are shown in Fig. 2 so they can be presented on a logarithmic time scale for clarity. We note that, as confirmed by experiments using Newtonian fluids, all instrument-related transients associated with the rate jumps are relaxed within the first ~10 ms, such that the transients shown here are entirely due to evolution of the sample's mechanical properties.

The transient results shown in Fig. 2 follow trends characteristic of a thixotropic material and agree quantitatively with the observations of Dullaert and Mewis (2006). They are qualitatively similar to results by Armstrong et al. (2016a) for an analogous fumed silica in paraffin oil and polyisobutylene suspension. Comparison of these curves shows that there are different time scales for structure break down and structure build up, and that these processes depend on the rate of deformation during the process. Thus, the relaxation processes have timescales that vary with the sample's shear history as the underlying processes depend on the current state of the structure. Furthermore, there are vestigial viscoelastic signatures at early times, evident as non-monotonic time evolution, showing the material is not purely thixotropic in its response (Mewis and Wagner 2012; Dullaert, 2005; Dullaert and Mewis, 2006; Armstrong 2015).

The corresponding values of the objective function F_{OBJ} corresponding to the steady state and step up and step down transient flow fitting results, as well as the overall value, for the fits obtained with the parameter values shown in Table 1 are shown in Table 2. The MDT model does an excellent job of fitting the dominant features of the steady state experiments across the entire range of experimental conditions explored. Some quantitative differences are observed for some of the relaxation processes, although the overall fitting is still very compelling. Small qualitative differences are observed, for example in Fig. 2b&c, where viscoelastic effects are evident in the experimental data in the form of non-monotonic stress responses which the [resent model cannot accommodate.

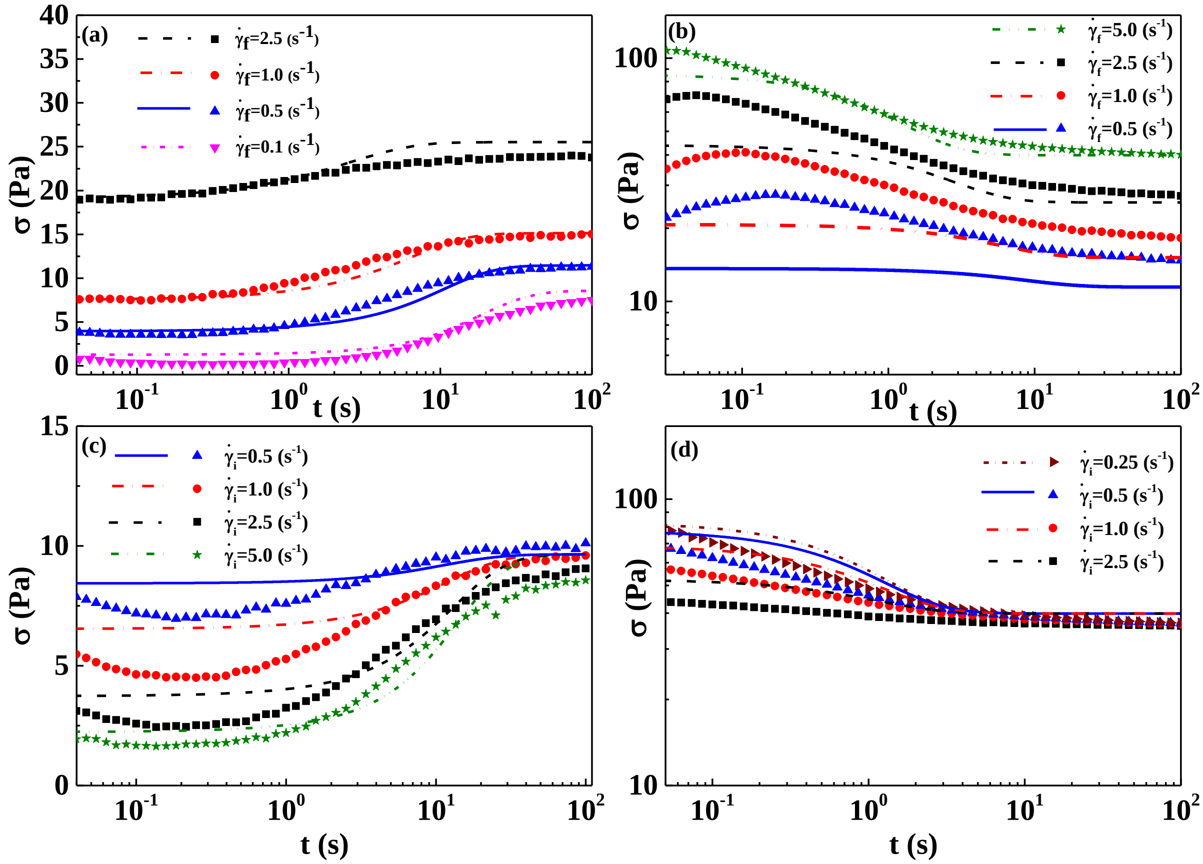

Fig. 2: (a) Data and MTM model fits of step down in shear rate from 5.0 (s^{-1}) to that listed in the legend; (b) Data and MTM model fits of step up in shear rate from 0.1 (s^{-1}) to that listed in the legend; (c) Data and MTM model fits of step down to 0.25 (s^{-1}) from shear rates listed in the legend; (d) Data and MTM model fits of step up to 5.0 (s^{-1}) from shear rates listed in the legend. In all plots, the discrete symbols and the lines represent the data and the corresponding model fits of the MTM model using the optimal fit parameters appearing in Table 1, respectively.

Table 2: F_{OBJ} of MDT fitting shown for the steady state data (SS), transient data (Trans) and overall average, λ

Description	MDTM
$F_{OBJ,\,SS}$	0.018
$F_{OBJ,\,Trans}$	0.100
$F_{OBJ,\,\mu}$	0.060

Structure predictions arising from the MDT model are shown in Fig. 3 (a-d) with each of these figures corresponding to the step up or step down experiments shown in Fig. 2(a-d). Using the structure prediction for the steady state flow curves for reference as shown in Fig. 1a the MDT model predictions for structure evolution during these transient tests can be seen to follow logical trends. Namely, the structure rebuilds upon lowering the applied shear rate, leading to increases of the structure viscosity and yield stress and vice versa. Furthermore, note that the structure evolution is always predicted to be monotonic during these processes, as the model currently does not incorporate viscoelasticity.

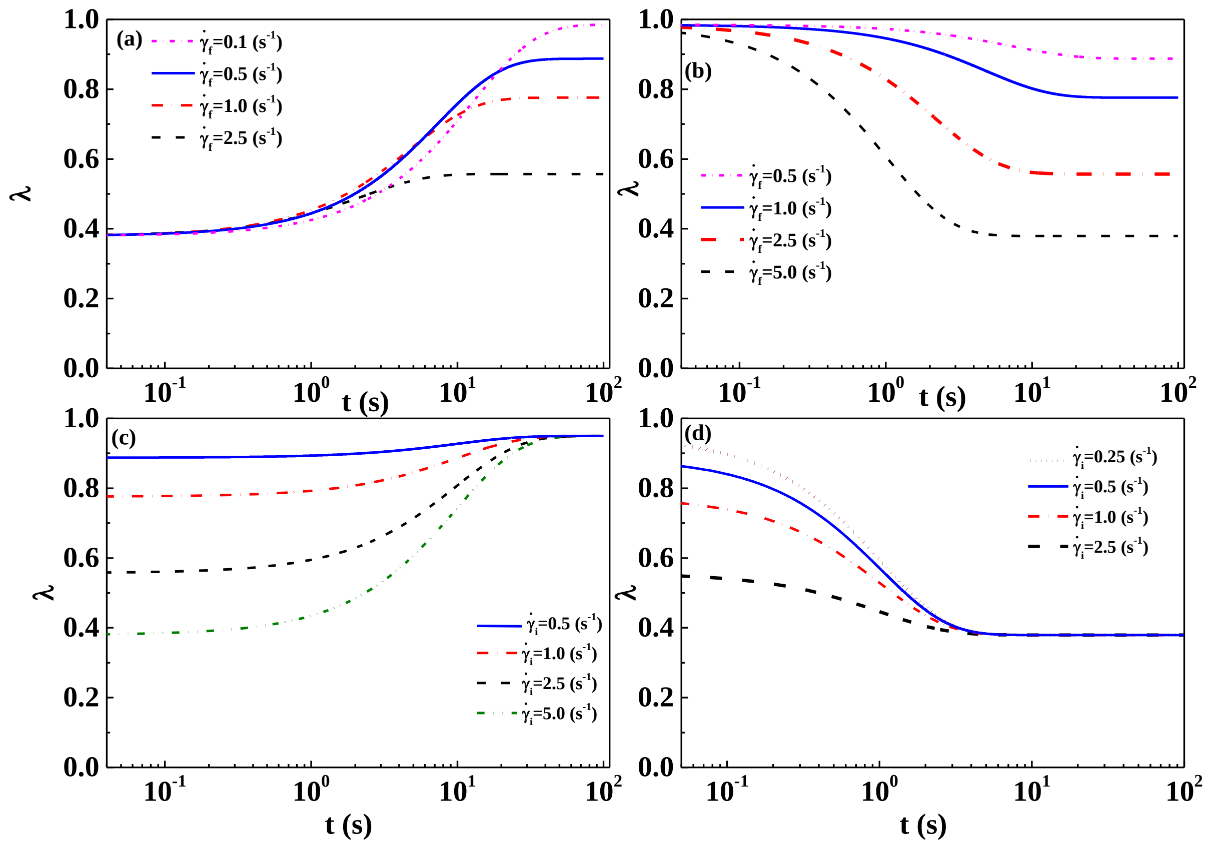

Fig. 3: (a) Structure predictions of step down in shear rate from 5.0 (s^{-1}) to that shown in the legend; (b) Structure predictions of step up in shear rate from 0.1 (s^{-1}) to that shown in the legend; (c) Structure predictions of step down to 0.25 (s^{-1}) from that shown in the legend respectively (in this data the initial shear rates are the same while the final shear rates vary); (d) Structure predictions of step up to 5.0 (s^{-1}) from that shown in the legend respectively (in this data the final shear rates are the same while the initial shear rates vary); all MDT model predictions are calculated with the parameter values "optimal" listed in Table 1.

In summary, let us highlight some key comparisons of the MDT model to the experimental data sets presented so far. Not surprisingly, the model has more than enough parameters to accurately model the steady state flow curve, as shown in figure Fig. 1a. Examination of the step-down and step-up in shear rate fitting in Fig. 2 shows that the MDT model can fit the data well, except for the nonmonotonic stress response at shorter times, which is characteristic of viscoelasticity. In Fig. 4 below we show expanded views of a step-down and a step-up experiment to enable a clearer view of the comparison. In Fig. 4a it is observed that the model generally is able to capture the main features of the data, while in Fig. 4b we see that someone of the subtleties of the material response, namely the stress overshoot, are missed and the model predicts a smaller value of the final stress along with a faster time constant for achieving steady state.

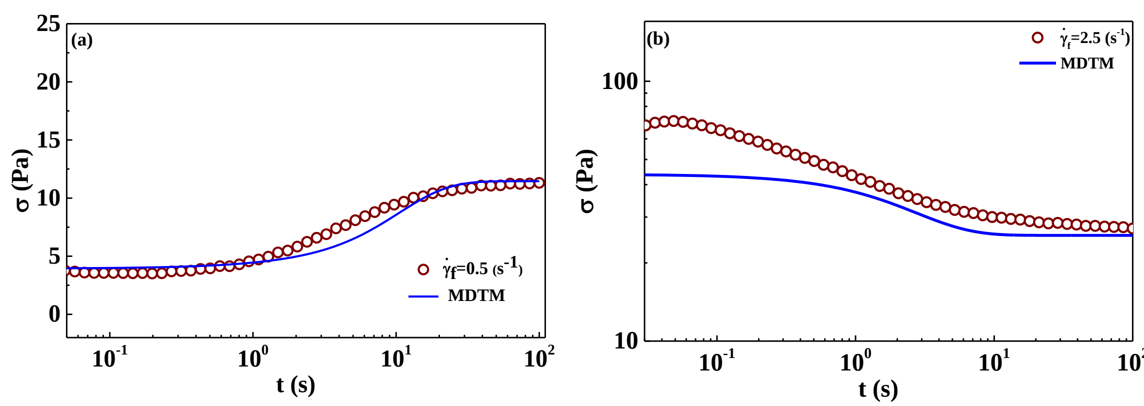

Fig. 4: (a) Close up of step-down in shear rate from 5.0 (s^{-1})to 0.5 (s^{-1}) data with MDT model fit; (b) Close up of step-up in shear rate from 0.1 (s^{-1}) to 2.5 (s^{-1}) with MDT model fit. (Armstrong 2015; Armstrong et al. 2016a)

What is apparent from these comparisons to experimental data under time dependent nonlinear shear flow is that accurate constitutive models for nearly ideal thixotropic materials, such as carbon black suspension investigated here, require a dominant viscous, and perhaps viscoelastic, response that is coupled to a time and rate dependent structure, and a structure parameter that can model it. In the next section, we compare *predictions* of one of these models, the MDT model, against various additional time-dependent flows that are used for characterizing thixotropic materials (i.e. LAOS and UD-LAOS).

LAOS Data and Predictions Using the MDT Model

The purpose of this section is to present LAOS data and compare them against the predictions of the MDT model using the best fit parameters from Table 1. The experimental LAOS results are shown in Fig. 5a&b in dimensionless form for convenience of comparison. The LAOS data shown in Figs. 5a and 5b are obtained at an angular velocity $\omega = 0.1\,(\mathrm{rad/s})$ and $\omega = 1\,(\mathrm{rad/s})$, respectively, over a range of strain amplitudes: $\gamma_0 = 0.1\text{-}100$. During the LAOS flow regime the strain rate is oscillatory

$$\gamma = \gamma_0 \sin(\omega t)\,, \tag{10}$$

where ω is the frequency and γ_0 is the strain amplitude., while the shear rate, as the first time derivative of strain, is given as

$$\dot{\gamma} = \omega\gamma_0 \cos(\omega t)\ . \tag{11}$$

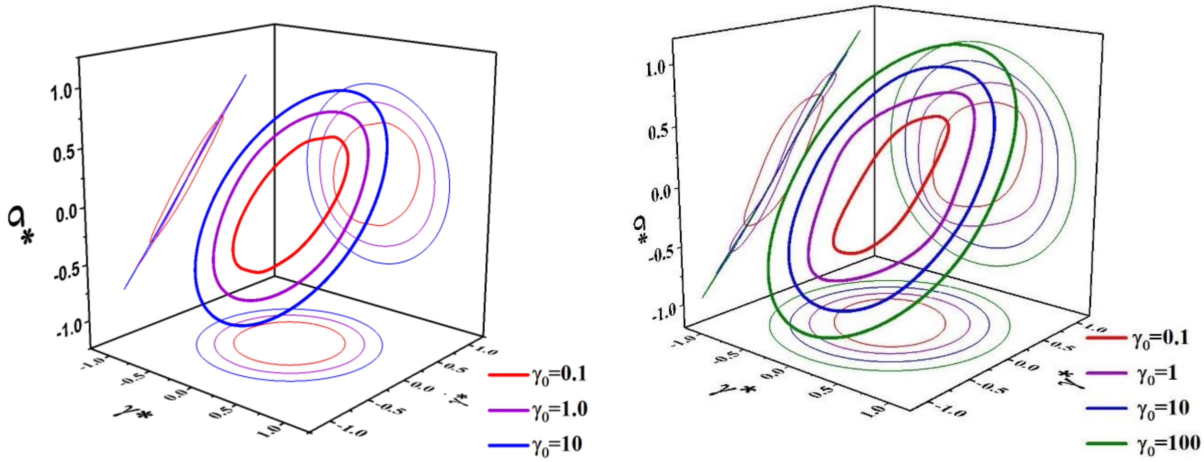

(a) $\omega = 0.1(\mathrm{rad/s})$ (b) $\omega = 1(\mathrm{rad/s})$

Fig. 5: LAOS data at (a) $\omega = 0.1(\mathrm{rad/s})$ and (b) $\omega = 1(\mathrm{rad/s})$ over a range of γ_0 values, as indicated in the figure, normalized by maximum values, then normalized stress values scaled by 0.5, 0.67, 0.83, and 1 for γ_0 =0.1; 1; 10; and 100 (left and right figure), respectively, for plotting purposes).

In Figs. 6 and 7 we compare the predictions of the MDT model to the experimental LAOS data at ω =1 (rad/s) for two different strain amplitude values, γ_0 =0.1 and 10, respectively. The comparisons are made using both the elastic projection (stress vs. strain: Figs. (b) and (d)) and the viscous projection (stress vs. shear rate: Figs. (c) and (e)) of the three-dimensional Lissajous-Bowdich curves (Fig. (a)). The series of depictions in both Fig. 6a-e and Fig. 7a-e all show how the stress and structure evolve over a complete cycle of LAOS at alternance, where the demarcations in the figures indicate analogous stages of the flow. As it can be seen in those figure, the MDT model provides semi-quantitative predictions at the higher strain amplitude. At the lower strain amplitude the MDT model predictions deviate significantly from the experiments, albeit still capturing the global features characteristic of probing the yield stress of the suspension. Additional LAOS elastic and viscous projections are shown for one more combination of strain amplitude and frequency in Fig. S.3 in Supplemental Material. One can see the reduction in shear rate, =that corresponds with the building of structure, albeit with some structural lag time. This trend is evident for all LAOS flow with the carbon black in napthenic oil.

As a measure of the quality of the model predictions we offer in Table 3 the objective functions calculated from the time-average of the square of the difference between the model predictions and the LAOS data for different strain amplitudes at $\omega = 1\,(\text{rad}/\text{s})$. As we can see from the results presented in that table, the quality of the predictions deteriorates as the strain amplitude decreases below approximately 1. We can again speculate that under those conditions viscoelastic effects, not captured by the MDT model, are responsible for most of the observed discrepancies.

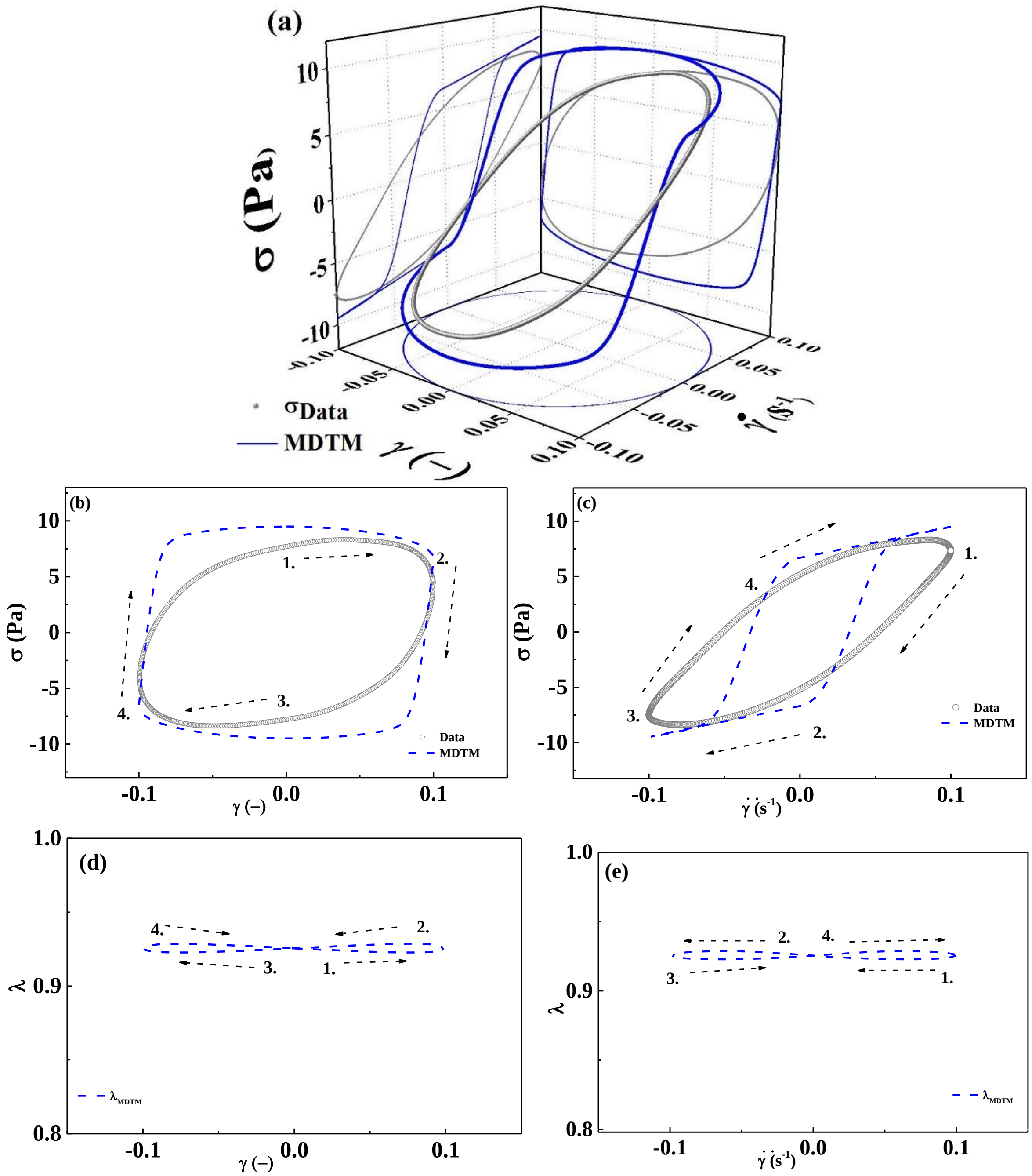

Fig. 6: (a) Three dimensional Lissajous–Bowditch curve $\omega = 1\,(\mathrm{rad/s})\,;\gamma_0 = 0.1$; (b) two dimensional elastic projection; (c) two dimensional viscous projection; (d) two dimensional structural, elastic projection; and (e) two dimensional structural viscous projection. The arrows indicate the direction of time evolution during the cycle and the numbers correspond to specific states discussed in the text. (Using respective best fit parameters in Table 1) (Armstrong 2015; Armstrong et al. 2016)

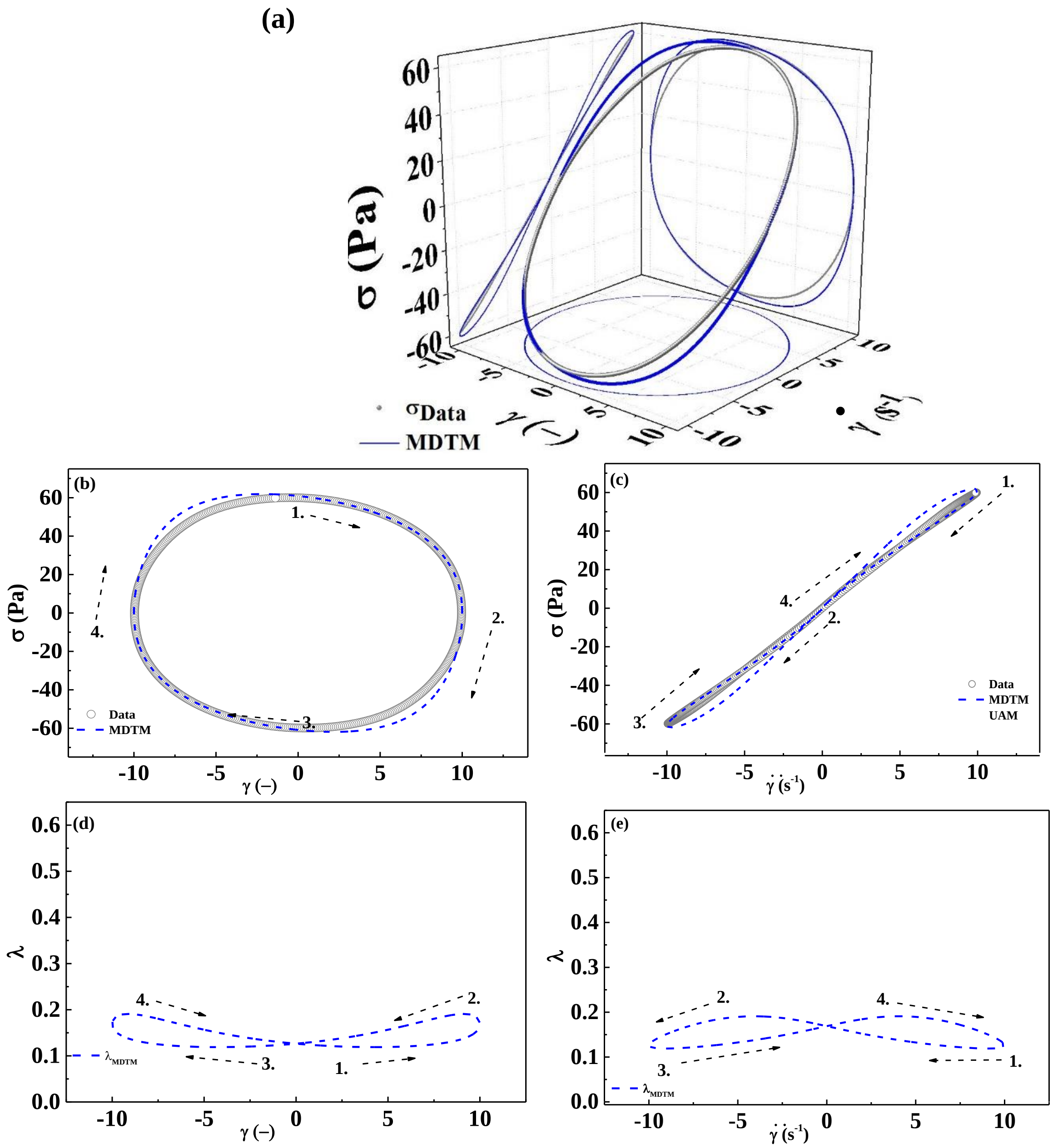

Fig. 7: (a) Three dimensional Lissajous–Bowditch curve $\omega = 1\,(\mathrm{rad/s}); \gamma_0 = 10$; (b) two dimensional elastic projection; (c) two dimensional viscous projection; (d) two dimensional structural, elastic projection; and (e) two dimensional structural viscous projection. The arrows indicate the direction of time evolution during the cycle and the numbers correspond to specific states discussed in the text (using best fit parameters indicated in Table 1).

Table 3: Quantitative estimates of the L_2 error norms corresponding to MDT model predictions of LAOS data at $\omega = 1\,(\mathrm{rad/s})$

ω=1 (rad/s)	γ_0 = 0.1	γ_0 = 1.0	γ_0 = 10	γ_0 = 100	Ave. F_{OBJ}
MDTM	**2.18**	**0.48**	**0.19**	**0.21**	**0.76**

In Fig. 8 all of the Lissajous-Bowditch two dimensional elastic and viscous projections are shown along with the MDT model predictions. From there one sees that as the structure is more and more broken down at higher strain amplitude and/or higher frequency, the stress becomes more and more viscous while it becomes more elastic at the inverse conditions. It can then be said that the MDT model is better able to capture the fluid behavior when viscous effects dominate.

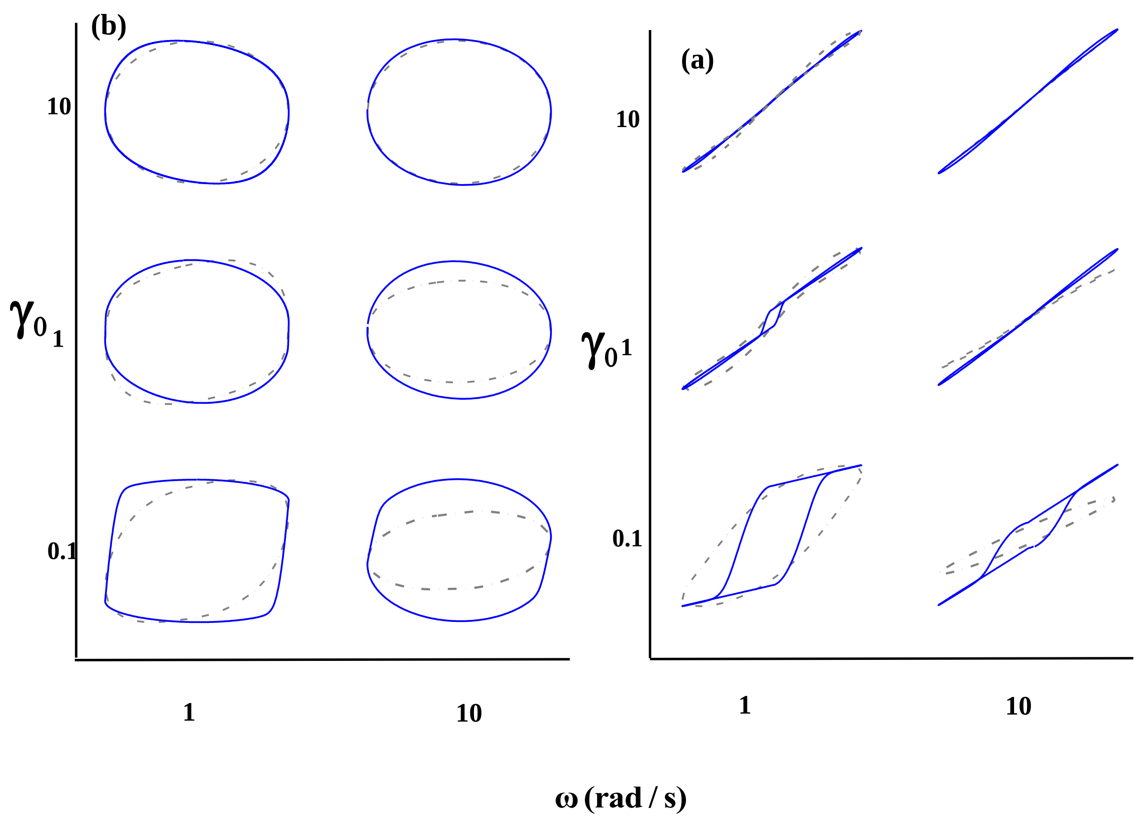

Fig. 8: Pipkin diagram: (a) Elastic projections. (b) Viscous projections. Data (gray open circles) and MDT model predictions (blue lines) using best fit parameters indicated in Table 1. The data are made dimensionless by maximum values, while the model predictions are made dimensionless by the same maximum values used for the data.

Flow Reversal and UD-LAOS Experiments and MDT Model Predictions

We now show the experimental data and model predictions under flow reversal and UD-LAOS conditions to further probe the model strengths and weaknesses. As previously observed (Dullaert and Mewis 2006; Mewis and Wagner 2012; Armstrong et al. 2016a) a structural kinetic model such as the MDT cannot capture well the changes induced upon flow reversal. We believe that this is because, as shown in Fig. 9, the MDT (as well as any other similar structural kinetic model) does not show any structural changes upon a reversal of sign in the shear rate. It is clear that some additional, presumably irreversible, structural changes induced due to such a change in the flow direction as implied in flow reversal experiments, need to be considered in future models. This model deficiency may also be responsible for the previously noted deficiencies in predicting well LAOS behavior, especially under conditions under which structural effects dominate.

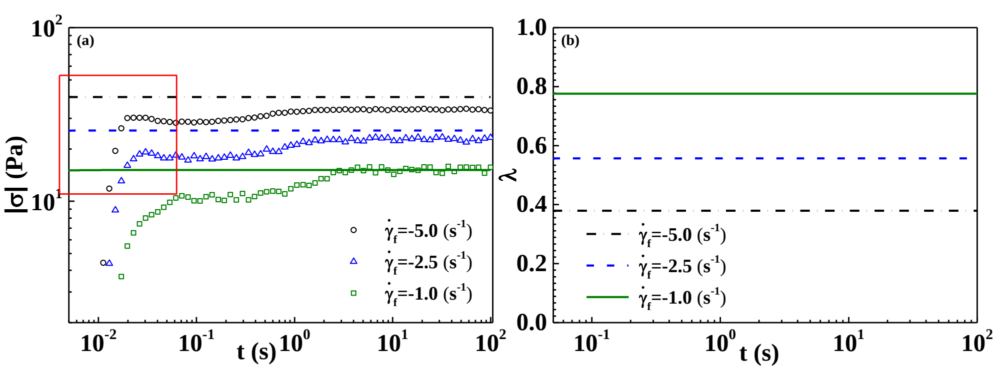

Fig. 9: (a) Flow reversal data with MDT model prediction of stress relaxation from three shear rates shown in figure; (b) Corresponding structure parameter predictions using the MDT model. The MDT model predictions have been obtained using best fit parameters indicated in Table 1.

Recently, Armstrong et al. (2016a) proposed a new way to perform LAOS, as a superposition to simple steady shear flow with the same magnitude as the amplitude of the shear rate used in the LAOS experiment. In this way, the flow moves in one direction only while still allowing for an oscillatory motion on top of the steady one. Thusly Eq. (10) and Eq. (11) now become Eq. (12) and Eq. (13) respectively,

$$\gamma = \gamma_0 \sin(\omega t) + \gamma_0 \omega t\,, \tag{12}$$

$$\dot{\gamma} = \omega\gamma_0 \cos(\omega t) + \omega\gamma_0\,. \tag{13}$$

More details about this type of flow can be found in (Armstrong et al. 2016a).

Sample UD-LAOS results are shown in Fig. 10 for similar conditions as the LAOS results presented in Fig. 8. To make these comparisons, the experimental data and model predictions are made dimensionless by first resolving the oscillating component of the stress in the alternance state by subtracting out the average stress, which is not zero in UD-LAOS, and then plotting the experimental data and corresponding model predictions scaled by the magnitude of the oscillating component of the stress as σ^* (Armstrong 2015; Armstrong et al. 2016a). The strain and shear rate are also calculated for the oscillating component and made dimensionless accordingly.

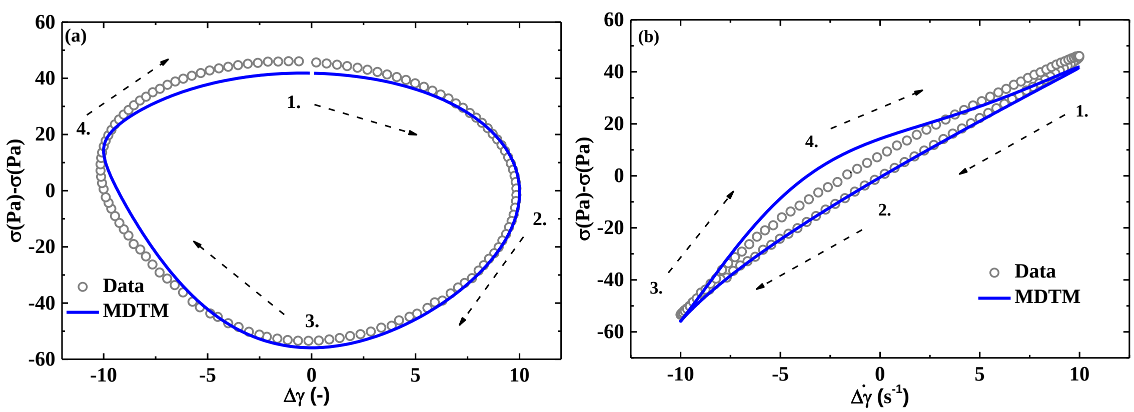

Fig. 10: UD-LAOS data compared to MDT model predictions obtained with the parameters of Table 1: (a) Elastic projections and (b) viscous projections $\omega = 1\,(\mathrm{rad/s})$; $\gamma_0 = 10$, where $\Delta\sigma = \sigma(t) - \bar{\sigma}(t)$ and $\bar{\sigma}(t) = 53.6\,(\mathrm{Pa})$, $\Delta\gamma = \gamma(t) - \omega\gamma_0 t$, and $\Delta\dot{\gamma} = \dot{\gamma}(t) - \omega\gamma_0$.

It is apparent from Fig. 10 that the symmetry of the LAOS curves in these projections is broken by the underlying steady base flow such that states 1-4 are now fundamentally different. The base flow is in the positive direction such that the applied shear rate at state 1 is actually twice that for the corresponding LAOS flow, while that of state 3 is zero. Thus, states 2 and 4 both correspond to states shearing instantaneously with the bulk shear flow, but state 2 is arrived at from a higher shear rate, with less structure, while state 4 is reached from a lower shear rate, with more structure (Armstrong 2015; Armstrong et al. 2016a). Correspondingly, the stress in state 2 is lower than that in state 4 due to a lower degree of structure that has not recovered as much as observed in state 4. Following the cycle from state 1 influenced by the base flow corresponds to transient reduction in the applied shear rate and a corresponding increase in the structure. The applied shear goes to zero at state 4 and the sample is once again undergoing positive shear rate such that the recovering structure is now subject to shear break down as well as shear aggregation (Armstrong 2015; Armstrong et al. 2016a). There is a similarity of UD-LAOS to traditional thixotropic loop tests where the shear rate is ramped up and down in the same direction and the stress reported. An important difference is that UD-LAOS probes a material at alternance rather than a material starting from rest (Armstrong 2015; Armstrong et al. 2016a). Additional UD-LAOS elastic and viscous projections shown in Fig. S.4 in Supplemental Material.

In Fig. 10 we compare predictions of the MDT model to experimental UD-LAOS data and UAM using the previously determined model parameters from fitting steady state, SAOS and step-up and step down transient shear experiments, as indicated in Table 1. In Table 4 we present the objective function contributions corresponding to the model predictions of UD- LAOS flows. Comparing these values against those corresponding to the LAOS experiments, shown in Table 3, shows that the model makes significantly more accurate predictions for UD-LAOS than for traditional LAOS flows. This confirms the importance of directionality of flow in models that incorporate a structure parameter in accordance with previous observations in the literature (Dullaert and Mewis 2006; Mewis and Wagner 2012; Armstrong 2015; Armstrong et al. 2016a).

Table 4: Quantitative estimates of the L_2 error norms corresponding to MDT model predictions of UD-LAOS data at $\omega = 1\,(\mathrm{rad/s})$

ω=1 (rad/s)	**γ_0 = 1**	**γ_0 = 5**	**γ_0 = 10**	**μ_{FOBJ}**
MDT	**0.06**	**0.04**	**0.04**	**0.05**

Strain-Rate Frequency Superposition Predictions

Soft matter with yield stress has long relaxation modes that complicate material characterization. Here, we use our thixotropy model, with the set of best fit parameters shown in Table 1, to test the proposed method of constant strain-rate dynamic oscillatory rheology (Wyss et al. 2007). Wyss et al. proposed characterizing such materials by performing a set of experiments with varying strain amplitude and frequency, but with a constant value of the product of strain amplitude and frequency. Furthermore, he proposed that a series of these curves, with the appropriate transformation applied would superimpose on each other to yield a master curve for the material at that value of the strain rate. In Fig. 11a, we provide predictions of this experiment by the MDT Model using the parameters shown in Table 1.

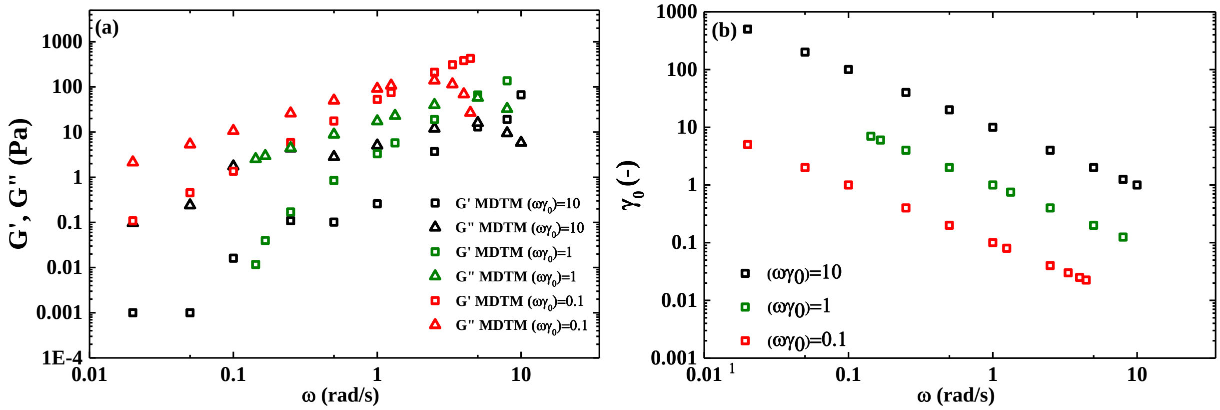

Fig. 11: (a) MDT model predictions for Frequency dependent storage $G'(\omega)$ (open squares) and loss modulus $G''(\omega)$ (open triangles) predictions at three different strain-rate amplitudes, $\dot{\gamma}_0$ shown in (b) (Wyss et al. 2007).

The scaled predictions are shown in Fig. 12, along with 2 sets G' and G" measurements from our experimental LAOS data represented by blue open pentagons and filled stars, respectively. We present the model predictions and data in this format to stay consistent with the original work of Wyss et al. (2007), as an additional method to show the MDT model's predictive capability. We acknowledge that experimentally the Wyss et al. technique should only defined for the regime of small amplitude oscillatory shear flow, where the microstructure is not disturbed, and the strain amplitudes are kept low. As proposed, the model predictions superimpose well, within the accuracy of the MDT model, and the data follows these trends. The values of strain rate amplitudes along with the shift factors a_s, and b_s are shown in Table 5.

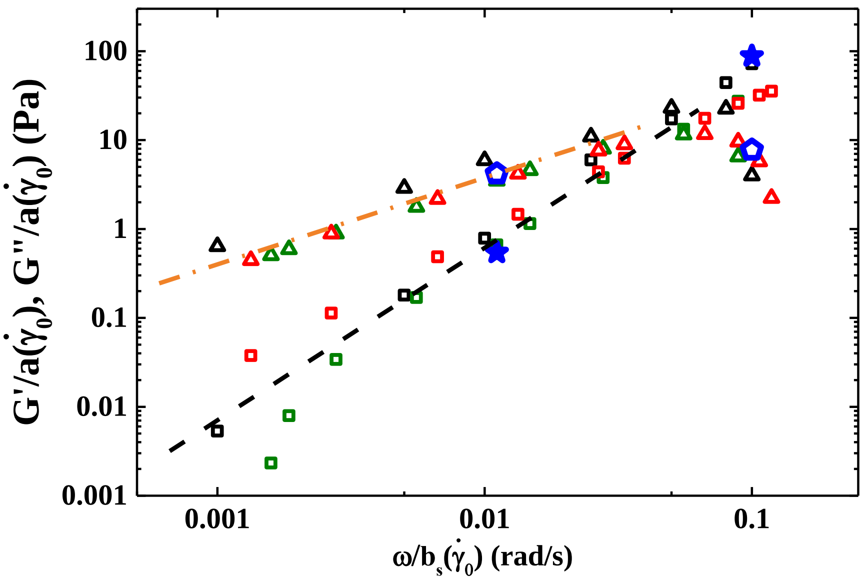

Fig. 12: Scaled experimental data and MDT model predictions of the constant frequency sweep measurement for G' and G" shifted onto a single master curve following (Wyss et al. 2007). The open pentagon and closed star symbols represent the experimental data for G' and G", respectively. The rest of the symbols follow the definitions shown in Fig. 11. The dashed lines show the trends.

Table 5: Wyss dimensionless plot shift factors, a_s and b_s for master curve (Wyss et al. 2007) as a function of $\dot{\gamma}_0 = \gamma_0\omega$, fit from the data presented in Fig. 11.

$\gamma_0\omega$ (s^{-1})	a_s	b_s
10	0.75	100
1	5	90
0.1	12	37.5

Our modeling provides a foundation for the proposal of Wyss et al. (2007) as follows. Holding the shear rate constant should, to first order, yield similar levels of microstructure in the material, and hence, this method attempts to characterize the material with a given level of structure. Such ideas have been proposed previously (for a review, see Mewis and Wagner, 2012). To illustrate this, model predictions for the level of structure are shown in Fig. 13, where for a constant $(\gamma_0\omega)$ there are relatively similar values of λ_{min} and λ_{max} corresponding to the experiments. Table 6 shows the ranges for λ_{min} and λ_{max} for three different combinations of strain amplitude and frequency for the three different values of constant $(\gamma_0\omega)$ used in this manuscript.

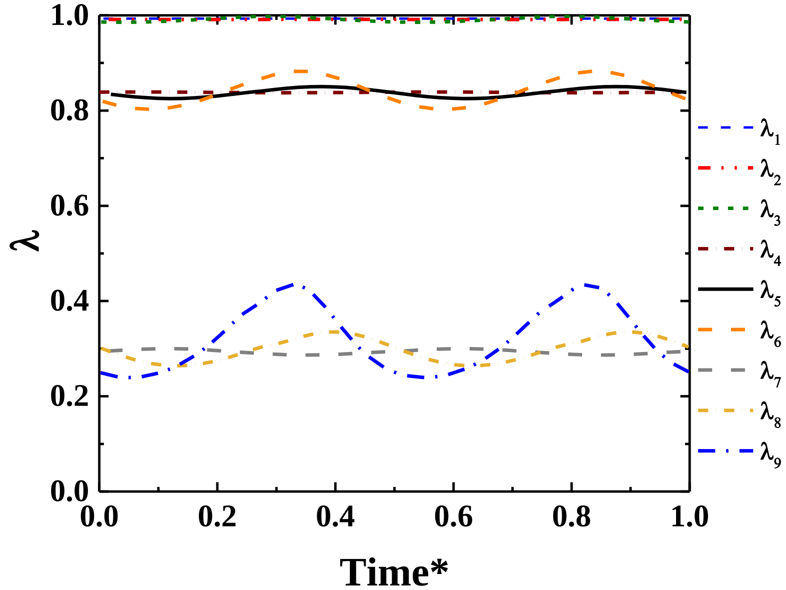

Fig. 13: λ vs. normalized time (normalized by length of period) for three sets of strain amplitude and omega products, for three different values of $(\gamma_0\omega)$. Details of each curve shown in Table 6, where runs (1-3), (4-6), and (7-9) correspond to shear rates of 0.1, 1, and 10 1/s respectively

In addition to the minimum and maximum structure level for each set of strain amplitude and angular frequency Table 6 shows the average structure value, and standard deviation for each strain amplitude frequency combination. From this table, it is evident that as the product of strain amplitude and frequency increases the magnitude of the structure minimum and maximum increases slightly. The average structure values are reasonably the same for a given value of the maximum shear rate. Thus, the structure predictions of the MDT model show that at constant values of the product of strain amplitude and frequency, the average level of structure is reasonably constant, and hence, the rheological characterization is of a material with this structure. The superposition shift factors then yield how the longest relaxation time shifts with varying levels of structure. This analysis now provides a mechanistic understanding of the hypothesis of Wyss et al. (2007).

Table 6: Lambda minimum and maximum comparisons (μ = average; σ = standard deviation

			λ		
γ_0	**ω [rad/s]**	**$\gamma_0\omega$ [1/s]**	**min**	**max**	**no.**
20	**0.5**	**10**	**0.240**	**0.430**	λ_9
5.5	**1.81**	**10**	**0.260**	**0.340**	λ_8
1	**10**	**10**	**0.280**	**0.300**	λ_7
		μ:	**0.26**	**0.34**	
		σ:	**0.015**	**0.039**	
			λ		
γ_0	**ω [rad/s]**	**$\gamma_0\omega$ [1/s]**	**min**	**max**	**no.**
7	**0.14**	**1**	**0.803**	**0.883**	λ_6
2	**0.5**	**1**	**0.820**	**0.850**	λ_5
0.0125	**8**	**1**	**0.830**	**0.840**	λ_4
		μ:	**0.82**	**0.85**	
		σ:	**0.01**	**0.02**	
			λ		
γ_0	**ω [rad/s]**	**$\gamma_0\omega$ [1/s]**	**min**	**max**	**no.**
5	**0.2**	**0.1**	**0.98**	**0.99**	λ_3
0.1	**1**	**0.1**	**0.99**	**0.991**	λ_2
0.0255	**4.44**	**0.1**	**0.993**	**0.993**	λ_1
		μ:	**0.99**	**0.99**	
		σ:	**0.004**	**0.001**	

Conclusions

New experimental data for a model thixotropic suspension of Carbon black system are presented that significantly extend the data set of Dullaert and Mewis to include LAOS, flow reversal, and novel unidirectional (UD-LAOS) flows, which are shown to be critically important for rigorously testing models for thixotropic suspensions (Dullaert 2005; Dullaert and Mewis 2006; Mewis and Wagner 2009; Mewis and Wagner 2012; Armstrong 2015; Armstrong et al. 2016). The experimental data set shows very little evidence of a viscoelastic response and is reproducible from batch to batch and between laboratories. A very rich LAOS behavior is observed when viscous stress and yield stress contributions are relevant that can is suggestive of a time-varying structure during alternance. The Modified Delaware Thixotropic (MDT) model (Armstrong 2015; Armstrong et al. 2016a) is found to robustly predict steady state, step-up and step-down in shear rate, SAOS, LAOS and the UD-LAOS experiments. The comparisons also highlight the difficulties of using LAOS experiments to determine model parameters for thixotropic materials. The thixotropic model is much more successful in predicting UD-LAOS, further confirming the importance of accounting for the induced anisotropy of structure in the advanced thixotropy models. Finally, the model and data are used to establish a foundation for the proposal of Wyss et al. (2007) for characterizing soft matter by holding the maximum shear rate fixed. This is shown to yield a rheological finger print at constant average structure, and subsequent superposition corresponds to correcting for how the maximum relaxation time changes with the level of structure. This study provides both new experimental data on a nearly ideal thixotropic system and demonstrates a robust, improved model with significant promise, but limitations on accuracy for LAOS flows, where the direction of flow changes.

Acknowledgements The authors acknowledge the support of the National Science Foundation through grant No. CBET 312146, the funding assistance from the U.S. Army, and the Department of Chemistry and Life Science, United States Military Academy. The views expressed herein are those of the authors and do not reflect the position of the United States Military Academy, the Department of the Army, or the Department of Defense.

References

Amari T, Watanabe K (1990) Flow properties and electrical conductivity of carbon black-linseed oil suspension. J Rheol 34:207-221

Aoki Y, Hatano A, Watanabe H (2003a) Rheology of carbon black suspensions. I. Three types of viscoelastic behavior. Rheol Acta 42:209-216

Aoki Y, Hatano A, Watanabe H (2003b) Rheology of carbon black suspensions. II. Well dispersed system. Rheol Acta 42:321-325

Aoki Y, Watanabe H (2004) Rheology of carbon black suspensions. III. Sol-gel transition system. Rheol Acta 43:490-395

Aoki Y (2011a) Rheology of carbon black suspensions. IV. Effect of suspending media on the sol-gel transition behavior. Rheol Acta 50:779-785

Aoki Y (2011b) Rheology of carbon black suspensions. V. Heat-induced gelation and its reversibility. Rheol Acta 50:787-793

Apostolidis AJ, Armstrong MJ, Beris AN (2015) Modeling of human blood rheology in transient shear flows. J Rheol 59:275-298

Armstrong MJ (2015) Investigating and modeling the thixotropic behavior, microstructure and rheology of complex material. Ph.D. Thesis, University of Delaware

Armstrong MJ, Beris AN, Rogers SA, Wagner NJ (2016a) Dynamic shear rheology of a thixotropic suspension: Comparison of an improved structure-based model with large amplitude oscillatory shear experiments. J Rheol 60:433-450

Armstrong MJ, Beris AN, Wagner NJ (2016b) An Adaptive Parallel Tempering Method for the Dynamic Data-Driven Parameter Estimation of Nonlinear Models. AIChE J. DOI 10.1002/aic.15577

Bird RB, Armstrong R, Hassager O (1987) Dynamics of Polymeric Liquids. John Wiley and Sons, NY

Blackwell B, Ewoldt RH (2014) A simple thixotropic-viscoelastic constitutive model produces unique signatures in large-amplitude oscillatory shear (LAOS). JNNFM 208-209:27-41

de Souza Mendes PR, Thompson RL (2012) A critical overview of elasto-viscoplastic thixotropic modeling. JNNFM 187-188:8-15

de Souza Mendes PR, Thompson RL (2013) A unified approach to model elasto-viscoplastic thixotropic yield-stress materials and apparent yield-stress fluids. Rheol Acta 52:673-694

Dimitriou CJ, Ewoldt RH, McKinley GH (2013) Describing and prescribing the constitutive response of yield stress fluids using large amplitude oscillatory shear stress (LAOStress). J Rheol 57:27-70

Dullaert K (2005) Constitutive equations for thixotropic dispersions. Ph.D. Thesis, Katholieke Universiteit Leuven

Dullaert K, Mewis J (2005a) Stress jumps on weakly flocculated dispersions steady state and transient results. J Colloidal and Interface Science 287:542-551

Dullaert K, Mewis J (2005b) A model system for thixotropy studies. Rheol Acta 45:23-32

Dullaert K, Mewis J (2006) A structural kinetics model for thixotropy. J Non-Newtonian Fluid Mech. 139(1-2):21-30

Germann N, Gurnon AK, Zhou L, Cook LP, Beris AN, Wagner NJ (2016) Validation of constitutive modeling os shear banding, threadlike wormlike micellar fluids. J. Rheol 60(5): 983-999

Goodeve CF (1939) A General Theory of Thixotropy and Viscosity. Trans. Faraday Soc. 35, 342–358

Hyun K, Wilhelm M, Klein CO, Kwang SC, Jung GN, Kyung HA, Seung JL, Ewoldt RH, McKinley GH (2011) A review of nonlinear oscillatory shear tests: Analysis and application of large amplitude oscillatory shear (LAOS). Progress in Polymer Science 36: 1697-1753

Larson RG (2015) Constitutive equations for thixotropic fluids. J Rheol 59:595-611

Metzner AB, Whitlock M (1958) Flow Behaviour of Concentrated (Dilatant) Suspensions. Trans. SOC. Rheol. 2, 239

Mewis J, Wagner NJ (2009) Thixotropy. Advances in Colloid and Interface Science 147-148: 214-227

Mewis J, Wagner NJ (2012) Colloidal Suspension Rheology. University Press, Cambridge, UK.

Mewis J, Wagner NJ (2012) Colloidal Suspension Rheology. Cambridge University Press, NY

Mujumdar A, Beris AN, Metzner AB (2002) Transient phenomena in thixotropic systems. J Non Newtonian Fluid Mech. 102:157-178

Osuji CO, Kim C, Weitz DA (2008) Shear thickening and scaling of the elastic modulus in a fractal colloidal system with attractive interactions. Phys. Rev. E 77:060402

Rogers SA, Erwin BM, Vlassopoulos D, Cloitre M (2011) Oscillatory yielding of a colloidal star glass. J. Rheol. 55(4): 733-752

Russel WB (1980) Review of the Role of Colloidal Forces in the Rheology of Suspensions. J. Rheol. 24, 287

Wyss HM, Miyazaki K, Mattson Z, Hu Z, Reichman DR, Weitz DA (2007) Strain-rate frequency superposition: a rheological probe of structural relaxation in soft materials. Physical Review Letters 98:1-4

Youssry M, Madec L, Soudan P, Cerbelaud D, Guyomard D, Lestriez B (2013) Non-aqueous carbon black suspensions for lithium-based redox flow batteries: rheology and simultaneous rheo-electrical behavior. Phys Chem Chem Phys 15: 14476-14486

Yearsley KM, Mackley MR, Chinesta F, Leygue A (2012) The rheology of mutiwalled carbon nanotube and carbon black suspensions. J Rheol 56:1465-1490